Induction of epithelial-mesenchymal transition (EMT) in breast cancer cells is calcium signal dependent

Felicity M. Davis[1,a], **Iman Azimi**[1], **Richard A. Faville**[2], **Amelia A. Peters**[1], **Kees Jalink**[3], **James W. Putney Jr**[4], **Geoffrey J. Goodhill**[2,5], **Erik W. Thompson**[6,7], **Sarah J. Roberts-Thomson**[1], and **Gregory R. Monteith**[1,*]

[1]School of Pharmacy, The University of Queensland, Brisbane, Australia [2]Queensland Brain Institute, The University of Queensland, Brisbane, Australia [3]Division of Cell Biology, The Netherlands Cancer Institute, Amsterdam, The Netherlands [4]Laboratory of Signal Transduction, National Institute of Environmental Health Sciences, Research Triangle Park, USA [5]School of Mathematics and Physics, The University of Queensland, Brisbane, Australia [6]St Vincent's Institute, Fitzroy, Australia [7]University of Melbourne Department of Surgery, St. Vincent's Hospital, Fitzroy, Australia

Abstract

Signals from the tumor microenvironment trigger cancer cells to adopt an invasive phenotype through epithelial-mesenchymal transition (EMT). Relatively little is known regarding key signal transduction pathways that serve as cytosolic bridges between cell surface receptors and nuclear transcription factors to induce EMT. A better understanding of these early EMT events may identify potential targets for the control of metastasis. One rapid intracellular signaling pathway that has not yet been explored during EMT induction is calcium. Here we show that stimuli used to induce EMT produce a transient increase in cytosolic calcium levels in human breast cancer cells. Attenuation of the calcium signal by intracellular calcium chelation significantly reduced epidermal growth factor (EGF)- and hypoxia-induced EMT. Intracellular calcium chelation also inhibited EGF-induced activation of signal transducer and activator of transcription 3 (STAT3), while preserving other signal transduction pathways such as Akt and extracellular signal regulated kinase 1/2 (ERK1/2) phosphorylation. To identify calcium-permeable channels that may regulate EMT induction in breast cancer cells, we performed a targeted siRNA-based screen. We found that transient receptor potential-melastatin-like 7 (TRPM7) channel expression regulated EGF-induced STAT3 phosphorylation and expression of the EMT marker vimentin. While intracellular calcium chelation almost completely blocked the induction of many EMT markers, including vimentin, Twist and N-cadherin, the effect of TRPM7 silencing was specific for vimentin protein

*Correspondence: Prof. G. Monteith, School of Pharmacy, The University of Queensland, Brisbane, Australia. Tel: +61-7-3346-1855; Fax: +61-7-3346-1999; gregm@uq.edu.au.
aCurrent address: Laboratory of Signal Transduction, National Institute of Environmental Health Sciences, Research Triangle Park, USA

CONFLICT OF INTEREST

The authors declare no conflict of interest.

expression and STAT3 phosphorylation. These results indicate that TRPM7 is a partial regulator of EMT in breast cancer cells, and that other calcium-permeable ion channels are also involved in calcium-dependent EMT induction. In summary, this work establishes an important role for the intracellular calcium signal in the induction of EMT in human breast cancer cells. Manipulation of calcium signaling pathways controlling EMT induction in cancer cells may therefore be an important therapeutic strategy for preventing metastases.

Keywords

Epithelial-mesenchymal transition (EMT); calcium; vimentin; STAT3; signal transduction; breast cancer

INTRODUCTION

Epithelial-mesenchymal transition (EMT) converts epithelial cells to a mesenchymal-like phenotype and is associated with the loss of cell contacts, production of the type-III intermediate filament protein vimentin, and increases in cell migration and invasion (1). This phenotypic switch is important during embryonic development and for pathological processes including the metastasis of solid tumors from the primary site to a secondary organ (2, 3). In addition to increases in the expression of classic EMT markers including Snail, Twist, vimentin and N-cadherin, EMT in breast cancer cells is associated with the evasion of apoptosis and senescence, and anoikis resistance (3, 4). Expression of EMT markers is a feature of the basal and claudin-low breast cancer subtypes, which have a poor clinical prognosis (5–8), and has been associated with breast cancer stem cell activity (9). EMT markers are also enriched in cancer cell populations surviving hormonal or cytotoxic therapy (10).

Many studies have investigated the molecular and cellular changes that occur as a consequence of EMT and how these changes may facilitate cancer cell dissemination and metastasis (9, 11). Comparatively little is known about key signal transduction pathways that govern the *induction* of EMT (12). In this study we used EGF and hypoxia to induce EMT in MDA-MB-468 human breast cancer cells. EGF-mediated activation of the EGFR produces a rapid and transient phosphorylation of multiple downstream signaling proteins, and a STAT3-Twist signaling pathway has been implicated in EGF-induced EMT in these cells (13). Therapeutic targeting of specific signaling pathways that regulate epithelial-mesenchymal plasticity may offer a novel approach for the prevention of cancer metastasis by inhibiting cellular conversions at the primary and/or secondary site. Identification of early signaling events important for EMT induction may aid in the development of clinically useful anti-metastatic therapies due to the inherent difficulties with targeting the transcription factors already identified as EMT regulators (14).

The calcium signal is a mechanism well suited to the rapid translation of signals from the tumor microenvironment into cellular responses (15–17). However, most studies investigating a role for calcium signaling in cancer have focused on processes important for the growth of the primary tumor (i.e. cell proliferation and apoptosis). For example, inhibition of calcium-permeable TRPC3 channels, which are elevated in clinical epithelial

ovarian cancer samples, reduces the proliferation of SKOV3 ovarian cancer cells (18). Calcium signaling is also important in the context of cancer cell migration and invasion (reviewed in Ref 19). Examples of calcium-dependent migratory processes are evident in prostate cancer cells, where silencing of the non-selective cation channel TRPV2 inhibits cell migration, an effect likely attributable to a reduction in basal cytosolic calcium concentrations (20). Pharmacological inhibition of store-operated calcium entry or silencing of components of this calcium influx pathway (ORAI1 and STIM1) in invasive MDA-MB-231 breast cancer cells inhibits cell migration, in-part through regulation of focal adhesion turnover (21). We have previously characterized changes in non-stimulated and store-operated calcium entry that occur as a *consequence* of EGF-induced EMT (22), and other studies have shown enhanced store-operated calcium entry associated with transforming growth factor-β (TGFβ)-induced EMT in breast cancer cells (23). In these studies we sought to determine the role of calcium signaling in the *induction* of EMT in breast cancer cells and to define the mechanisms involved.

RESULTS

Scratch-wounding initiates an intracellular calcium wave in breast cancer cells

Mechanical wounding promotes a migratory cell phenotype and induces the mesenchymal marker vimentin in breast epithelial cells (24). To assess possible rapid changes in calcium signaling as a consequence of wounding we scratched a confluent monolayer of MDA-MB-468 human breast cancer cells. An immediate increase in free cytosolic calcium ($[Ca^{2+}]_{CYT}$) in cells adjacent to the scratch and the propagation of an intracellular calcium wave emanating from the wound site was observed (Fig. 1A and Movie S1).

Quantitative analysis of scratch-induced calcium wave propagation was performed by fitting the dependence of the cell activation time (T_f) on distance from the wound edge (D) by $T_f = A*D^n$, where A and n are constants (Fig. 1B and Fig. S1). An n = 1 indicates propagation at a constant speed 1/A, while n = 2 indicates a purely diffusive process with a diffusion constant 1/A. The best-fitting value of n was 1.50 ($R^2 = 0.82$), suggesting a mixed model of calcium signaling following mechanical wounding that may involve intercellular communication via gap junctions as well as IP_3 receptor-mediated wave propagation, transitioning to a mechanism of calcium wave propagation that is likely to involve the release of a diffusible extracellular calcium-mobilizing agent. Support for a model of calcium wave propagation involving the release of an extracellular agent was given by the ability of conditioned media (from a scratched monolayer collected immediately after wounding) to promote vimentin protein induction mediated by EGF (Fig. 1C).

EGF stimulation produces an intracellular calcium signal and induces EMT in MDA-MB-468 breast cancer cells

EGF is a well characterised EMT inducer in MDA-MB-468 cells (12, 13, 25) and a factor known to be released in the tumor microenvironment (26). The ability of EGF to increase $[Ca^{2+}]_{CYT}$ in MDA-MB-468 breast cancer cells was therefore evaluated. EGF induced a transient increase in $[Ca^{2+}]_{CYT}$ (Fig. 1D and E). Activation of the protease-activated receptor 2 (PAR2) with trypsin and purinergic receptor activation with ATP also increased $[Ca^{2+}]_{CYT}$ (Fig. 1D and E). We then compared the ability of these agents to increase $[Ca^{2+}]_{CYT}$ with their ability to induce EMT, as assessed by increases in vimentin protein expression. PAR2 and purinergic receptor activation, despite producing significantly higher elevations in $[Ca^{2+}]_{CYT}$, failed to induce EMT in MDA-MB-468 cells (Fig. 1F). These findings are consistent with one of two scenarios—either EGF-induced EMT arises independently of calcium signaling or the nature (e.g., spatial and temporal aspects (27)) of the calcium signal elicited by EGF is of critical importance in the regulation of EMT induction.

Intracellular calcium chelation inhibits EGF-induced EMT

To directly explore a role for the calcium signal in the induction of EMT, MDA-MB-468 cells were pre-treated with the intracellular calcium chelator BAPTA-AM and the ability of EGF to induce vimentin expression in the absence of increases in $[Ca^{2+}]_{CYT}$ was assessed. A significant and pronounced decrease in EGF-induced vimentin expression was observed with intracellular calcium chelation (Fig. 2A). Induction of vimentin by EGF was also inhibited by another intracellular calcium chelator EGTA-AM (Fig. 2B).

Intracellular calcium chelation (BAPTA-AM) also blocked EGF-induced increases in mRNA levels of many EMT-associated genes, including vimentin (Fig. 3A and B), Twist (Fig. 3C and D) and N-cadherin (Fig. 3E and F). BAPTA-AM increased basal and EGF-induced Snail mRNA levels (Fig. 3G and H), indicating that calcium signaling may differentially regulate EMT-associated transcription factors in breast cancer cells. Intracellular calcium chelation also blocked EGF-mediated increases in the CD44/CD24 ratio (Fig. 3I and J). These effects were evident after treatment with EGF for six or 24 hours.

In addition, pre-treatment with BAPTA-AM strongly inhibited the cellular transformation from a grape-like to a spindle-like morphology with EGF-induced EMT (Fig. S2). However, BAPTA-AM did not appear to prevent the initial loss of cell-cell adhesions associated with EGF treatment (Fig. S2). Collectively these results demonstrate a critical role for Ca^{2+} signaling in EGF-induced EMT.

Intracellular calcium chelation inhibits hypoxia-mediated EMT

To assess whether calcium signaling was critically involved in other models of EMT induction we assessed the effect of intracellular calcium chelation on hypoxia-mediated EMT in breast cancer cells. Hypoxia-mediated increases in vimentin and N-cadherin mRNA levels and the CD44/CD24 ratio were also inhibited by intracellular calcium chelation in this model (Fig. 4A–C). Consistent with the EGF model, BAPTA-AM markedly increased Snail mRNA levels in these cells (Fig. 4D). Unlike EGF-induced EMT, Twist mRNA levels were

not affected by intracellular calcium chelation (Fig. 4E). These findings indicate that several elements of hypoxia-induced EMT are also blocked by intracellular calcium chelation.

STAT3 activation is calcium signal dependent

To define the molecular pathways involved in calcium-dependent modulation of EMT induction we assessed several EGF-mediated signaling events (13) in the presence and absence of $[Ca^{2+}]_{CYT}$ chelation. No significant alteration in EGF-induced phosphorylation of the EGFR (Tyr1173) was observed in cells pre-treated with BAPTA-AM (Fig. 5A–C). As this early EGF signaling event was intact in cells with intracellular calcium chelation, the inhibitory effects of BAPTA-AM must originate from calcium-dependent processes downstream of the EGFR.

A significant increase in EGF-induced ERK1/2 phosphorylation (Thr202/Tyr204) was apparent with intracellular calcium chelation (Fig. 5D–F). Basal intracellular free calcium levels have previously been shown to regulate the extent and duration of EGF-induced ERK1/2 phosphorylation (28), an effect that may be explained by calcium-dependent regulation of mitogen-activated protein kinase phosphatases (29). We then assessed the calcium dependence of Akt and STAT3, two key signal transducers that are also activated downstream of the EGFR. Calcium chelation failed to alter the degree of phosphorylation (Ser473) of Akt as a consequence of EGF stimulation (Fig. 5G–I). However, STAT3 phosphorylation (Tyr705) by EGF was substantially inhibited with intracellular calcium chelation (Fig. 5J–L). This effect was most pronounced at early (20 min) time points, where more than 90% of STAT3 phosphorylation was inhibited. These findings indicate that, while many elements of EGF signaling remain intact, chelation of intracellular calcium exquisitely inhibits the ability of cancer cells to undergo EMT in response to EGF, in-part through STAT3, which is a demonstrated driver of EMT in this (13) and other models (30).

siRNA mediated silencing of TRPM7 inhibits EGF-induced vimentin expression

To explore the identity of putative calcium channel(s) associated with EMT induction, we screened a panel of calcium influx channels for their ability to regulate EGF-induced vimentin expression. Channels assessed in this targeted immunofluorescence screen have previously been shown to regulate migratory or growth-factor mediated processes in epithelial cells (21, 31–34), and include the calcium release activated current (CRAC) channel pore subunit ORAI1, the transient receptor potential (TRP) vanilloid type-3 (TRPV3), canonical types (TRPC) 4, 5, 6 and the melastatin-like (TRPM) 6 and 7 channels. A significant decrease in EGF-induced vimentin induction was detected with TRPM7 siRNA in our immunofluorescence screen (Fig. 6A). This phenotype was confirmed with immunoblot assays of EGF-mediated vimentin induction with TRPM7 knockdown using two different types of siRNA (Dharmacon ON-TARGET*plus* and siGENOME, each consisting of a different pool of four rationally designed siRNAs; Fig. 6B–F), and using the TRPM7 channel inhibitor NS8593 (35) (Fig. 6G–H). However, TRPM7 silencing did not affect vimentin mRNA levels (Fig. S3), showing that it acts predominately at the protein level.

Given the effect of inhibiting TRPM7 expression (siRNA) or function (NS8593) on EGF-induced vimentin protein expression, we investigated whether TRPM7 channel expression affects the global cytosolic calcium response to EGF. No significant differences in the cytosolic calcium response to EGF stimulation were detected in MDA-MB-468 cells with TRPM7 siRNA versus the non-targeting siRNA control (Fig. S4A–C), indicating that modulation of vimentin protein induction by TRPM7 occurs independently of EGF-mediated increases in global cytosolic calcium levels. In addition, we assessed whether EGF directly activates TRPM7 channels (independently of the EGFR) using N1E-115 cells that stably express plasmalemmal TRPM7 channels but do not express the EGFR (36). EGF stimulation did not produce an increase in cytosolic calcium in these cells (Fig. S4D), demonstrating that EGF does not directly bind to and activate TRPM7 channels, as may occur with other ligand-gated TRP channels (e.g., TRPV1 (37)).

TRPM7 silencing attenuates EGF-induced STAT3 phosphorylation

To further delineate the role for TRPM7 in EGF-induced EMT we assessed the activation of downstream signal transduction pathways in cells with TRPM7 silencing. Consistent with the calcium chelation experiments, phosphorylation of the EGFR (Fig. 7A) and Akt (Fig. 7B) was not altered by TRPM7 silencing. However, in contrast to the induction seen with calcium chelation, a significant reduction in the phosphorylation of ERK1/2 was observed in breast cancer cells transfected with TRPM7 siRNA (Fig. 7C). This apparent reduction in ERK1/2 activation may be attributed to an increase in total ERK1/2 abundance with sustained TRPM7 silencing (Fig. 7C).

Due to the pronounced inhibition of STAT3 phosphorylation observed with intracellular calcium chelation (Fig. 5J–L), we next assessed the effect of TRPM7 silencing on EGF-induced STAT3 activation. Consistent with the calcium chelation experiments, a significant reduction in EGF-induced STAT3 phosphorylation was a consequence of TRPM7 silencing in MDA-MB-468 breast cancer cells (Fig. 7D). Thus, while TRPM7 regulates some elements of EGF-induced EMT (i.e. vimentin protein induction and STAT3 phosphorylation), EGF-induced increases in the mRNA levels of other EMT markers (i.e. Twist and N-cadherin) (Fig. S3), and EGF-induced changes in cell morphology (Fig. S5), are not affected by modulation of TRPM7, suggesting that other transporters of calcium are likely to be involved in the other aspects of calcium-dependent EMT induction demonstrated by calcium chelation.

DISCUSSION

Calcium is important for many physiological and pathological processes ranging from neurotransmission and cardiac contractility to cancer progression. There is now a general appreciation of the complexity of the calcium signal and its reliance on temporal and spatial characteristics as ways in which to define a cellular response (27). This work describes for the first time a mechanism whereby induction of EMT in human breast cancer cells is abrogated by intracellular calcium chelation.

Transient increases in $[Ca^{2+}]_{CYT}$ have been characterized in normal human urothelial cells post-wounding, with cells at the wound edge exhibiting sustained elevations in $[Ca^{2+}]_{CYT}$

(38). Our studies show that increases in $[Ca^{2+}]_{CYT}$ are also observed in breast cancer cells post-wounding. Mechanical wounding generated an intracellular calcium wave in MDA-MB-468 breast cancer cells that was propagated by the release of a diffusible extracellular calcium-mobilizing agent and via cell-cell communication. Conditioned media from scratched monolayers increased EGF-induced vimentin expression in MDA-MB-468 cells. Wound-like effects together with local elevations in EGF (or related ligands of the EGFR), both of which may occur at the edge of primary tumors *in vivo* (26, 39), could act to enhance the efficiency of EMT and tumor metastasis. The importance of local and coordinated signaling events is evident in intestinal epithelial cells where TGFβ and EGF work synergistically to induce an EMT-like phenotype (40).

EGF-induced EMT was calcium signal dependent, and the nature of the calcium signal was of critical importance. In MDA-MB-468 cells, EGF produced an immediate increase in $[Ca^{2+}]_{CYT}$ and an increase in vimentin protein expression after 24 h. Stimulation with other calcium mobilizing agents, including ATP and trypsin, failed to induce vimentin, despite producing large increases in free cytosolic calcium levels. The absence of an EMT-like phenotype with trypsin and ATP treatment indicates that calcium-dependent EMT may be regulated in a manner that is dependent on the spatial and temporal aspects of the signal, as distinct from magnitude-dependent increases in global $[Ca^{2+}]_{CYT}$.

A direct role for the calcium signal in EGF-induced EMT was demonstrated by the ability of intracellular calcium chelation to block increases in vimentin protein expression and the mRNA levels of several EMT-associated genes, including vimentin, Twist and N-cadherin. In contrast to other EMT markers, a significant increase in Snail mRNA was observed with intracellular calcium chelation. These findings suggest that the calcium signal differentially regulates EMT-associated transcription factors. However, the overall inhibitory effect of BAPTA-AM on EGF-induced EMT indicates that Snail is not a key transcription factor involved in EGF-induced EMT in MDA-MB-468 breast cancer cells, as suggested previously (13). Induction of the EMT markers vimentin and N-cadherin, and changes in the CD44/24 ratio, were also calcium-dependent in hypoxia-induced EMT, suggesting that the calcium signal may be exploited in a variety of pathways that lead to EMT.

The identification of the calcium-permeable ion channel TRPM7 as a partial regulator of EMT induction indicates that in addition to being involved in processes important for steering the directional migration of cells (31), TRPM7 is also involved in the induction of a more migratory and invasive phenotype through EMT. Recent work supporting this finding describes an association between TRPM7 levels and metastasis formation in human breast cancers (34). Given that TRPM7 silencing did not alter the global cytosolic calcium response to EGF, further studies are required to determine whether the effect of TRPM7 on EGF-induced vimentin protein expression and STAT3 phosphorylation is related to its calcium-transporting ability (i.e. local calcium signaling), or whether this phenotype may be attributed to a dysregulation of intracellular magnesium homeostasis or TRPM7 kinase activity (41). Although our results indicate that EGF does not directly bind to and activate TRPM7 channels, EGF may indirectly activate calcium influx through TRPM7 in MDA-MB-468 breast cancer cells via an EGFR-phospholipase C (PLC) signaling pathway, as previously shown for other PLC-coupled receptor agonists, including bradykinin and

thrombin (36). The inability of TRPM7 silencing to inhibit all of the aspects of EMT inhibited by Ca^{2+} chelation (BAPTA-AM) strongly suggests that other transporters of calcium are involved in specific aspects of calcium-dependent EMT induction.

The reduction in EGF-induced STAT3 phosphorylation by buffering of increases in $[Ca^{2+}]_{CYT}$, or (in-part) by silencing of TRPM7, provides further evidence for the importance of STAT3 in EMT-induction in MDA-MB-468 breast cancer cells (13). Growth factor mediated tyrosine phosphorylation of STAT3 by insulin-like growth factor-1 (IGF-1) in rat cardiomyocytes is calcium-dependent (42). In addition, cell adhesion-mediated STAT3 activity in NIH3T3 cells is reduced by chelation of extracellular calcium (to disrupt cell adhesions) (43). To our knowledge, this work is the first to report that EGF-mediated STAT3 activity in breast cancer cells is highly regulated by intracellular free calcium levels, and adds STAT3 to the list of known calcium-dependent transcription factors, which includes nuclear factor of activated T cells (NFAT) and nuclear factor kappa B, both of which are important in key aspects of cancer progression (44, 45).

In summary, we have identified a central role for the calcium signal in the induction of EMT in human breast cancer cells by multiple stimuli, and have shown that the nature of this calcium signal is of critical importance. Therefore, in addition to regulating processes important for metastasis, such as cell migration, invasion and apoptotic resistance (19), calcium signaling also regulates the ability of some stimuli to induce a more invasive phenotype. We have also shown that EGF-induced STAT3 phosphorylation is highly calcium-dependent and partially regulated by the calcium-permeable ion channel TRPM7. The targeting of calcium-dependent pathways that regulate EMT induction may therefore offer new therapeutic approaches for combating cancer metastasis.

MATERIALS AND METHODS

Cell culture

MDA-MB-468 cells were maintained in a humidified incubator (37°C) in Dulbecco's Modified Eagle's Medium supplemented with 10% fetal calf serum (FCS), 4 mM L-glutamine, 100 U/mL penicillin and 100 μg/mL streptomycin, as previously described (46). MDA-MB-468 cells routinely tested negative for mycoplasma infection (MycoAlert; Lonza, Basel, Switzerland) and STR profiling of the MDA-MB-468 cell line was performed by the Queensland Institute of Medical Research, using the StemElite ID Profiling Kit (Promega, Madison, WI, USA). N1E-115/TRPM7 cells were cultured as described previously (47). To induce EMT with EGF, MDA-MB-468 cells were serum starved (0.5% FCS, 24 h) and treated with 50 ng/mL EGF (E9644; Sigma Aldrich, St. Louis, MO, USA) (13), unless otherwise specified. For hypoxia-induced EMT, cells were exposed to a hypoxic insult (1% O_2) for six hours. Cells were then returned to normal culture conditions for six hours and RNA was isolated as described below (48, 49).

For studies assessing the ability of conditioned media to augment EGF-induced EMT, MDA-MB-468 cells were serum starved for 24 h. A pipette tip was used to scratch cell monolayers (50) and the media was aspirated. Cells were incubated with conditioned media or control (media from unscratched wells) for 30 min prior to EMT induction with EGF. For

studies assessing the ability of calcium-mobilizing drugs to induce vimentin, cells were serum starved and treated with EGF (50 ng/mL), trypsin (30 nM) or ATP (100 μM) for 24 h prior to immunofluorescence. For experiments involving the chelation of intracellular calcium, cells were loaded with 100 μM BAPTA-AM (B6769; Invitrogen, Carlsbad, CA, USA) or EGTA-AM (E1219) for 1 h at 37°C prior to stimulation with EGF (51).

Measurement of intracellular calcium

Measurement of intracellular calcium in MDA-MB-468 cells in response to EGF was performed with a fluorometric imaging plate reader (FLIPR[TETRA]; Molecular Devices, Sunnyvale, CA, USA) using the BD PBX no-wash Ca^{2+} Assay Kit (BD Biosciences, Franklin Lakes, NJ, USA) (52). Cells were loaded for 60 min at 37°C with 2 μM Fluo-4 AM (Invitrogen) in a solution containing 5% (v/v) PBX Signal Enhancer and 500 μM probenecid (Sigma Aldrich) in physiological salt solution (PSS; 10 mM HEPES, 5.9 mM KCl, 1.4 mM $MgCl_2$, 1.2 mM NaH_2PO_4, 5 mM $NaHCO_3$, 140 mM NaCl, 11.5 mM glucose, 1.8 mM $CaCl_2$) (22). Intracellular calcium measurements were performed with an excitation intensity of 470–495 nm and a 515–575 nm emission filter. Fluorescent values were normalized to the starting fluorescence and expressed as 'relative $[Ca^{2+}]_{CYT}$'. Pseudo-ratiometric calcium recordings in N1E-115/TRPM7 cells (36), were performed by loading cells plated on glass coverslips with Oregon Green BAPTA-1 488 AM (10 μg/mL) and Fura-Red AM (30 μg/mL) in HEPES buffered saline (HBS; 10 mM HEPES, 5 mM KCl, 1 mM $MgCl_2$, 140 mM NaCl, 10 mM glucose, 1.8 mM $CaCl_2$). Measurements were performed on a BioRad MRC600 confocal microscope, exciting at 488 nm and reading out Oregon Green (500–560 nm) and Fura-Red (580–650 nm) simultaneously. Data are presented as 'ratio OG/FR'.

For imaging the calcium response to mechanical wounding, MDA-MB-468 cells were plated in 96-well imaging plates and grown to confluency. Cells were loaded as previously described, with Fluo-4 AM, PBX signal enhancer and probenecid in HEPES-buffered DMEM. Confluent cell monolayers were wounded by scratching with a pipette tip (50). Images were acquired with a 20× objective using a Nikon Eclipse TE 300 inverted epifluorescence microscope (488 nm excitation and 550 nm emission). A 33 ms exposure time was used. Pseudocolor images were generated in ImageJ (v1.45b, National Institutes of Health (NIH)) with a 16-color LUT; brightness and contrast adjustment was uniformly applied to all images.

Quantitative analysis of scratch-induced calcium waves

For cell image segmentation a candidate image was generated representing the average of all movie frames subsequent to the scratch event (Fig. S1A). The outline of individual cells was determined by applying a watershed transformation to the candidate image (Fig. S1B) using the *MATLAB Image Processing Toolbox* (v7.11.0.584 (R2010b), The MathWorks, Natick, MA, USA). Cell groups with an average normalized pixel intensity < 0.2 and cell groups with an area ratio < 0.1 were excluded from the subsequent analysis.

The calcium transient for each cell was calculated as the average pixel intensity over all pixels within a given cellular region (Fig. S1C). The resulting calcium transients *I(T)* were fitted by a Boltzmann sigmoidal equation, which has the following functional form:

$$I(T)=I_0+\frac{I_A}{1+e^{-k(T-T_h)}} \quad (1)$$

where I_0 is the transient baseline, I_A is the transient amplitude, k is the slope factor, T is time and T_h is the half-activation time (see also Fig. S1D). The parameters from Eqn. (1) were fitted using the *lsqnonlin* function from the *MATLAB Optimization Toolbox*.

The time at which a cell group was activated, denoted by T_f, can be determined by rearranging Eqn. (1) as follows:

$$T=T_h - \frac{1}{k}\log_e\left(\frac{1}{\alpha}-1\right) \quad (2)$$

where α is the proportion of the calcium transient above baseline (i.e. $\alpha = (I - I_0)/I_A$). Cell groups were considered active when $\alpha = 0.5$, at which point T_f is given the equation 2.

The distance of the cell group relative to the location of the scratch was calculated as the perpendicular distance from the cell group's centroid to the line defining the scratch event. To determine the relationship between T_f and D, the following equation was fit to the firing time/distance tuples for each cell groups:

$$T_f=A \times D^n \quad (3)$$

where A is a scaling coefficient and n is a power law exponent. The parameters A and n from Eqn. (3) were fit using the *lsqnonlin* function from the *MATLAB Optimization Toolkit*.

Phase contrast microscopy

MDA-MB-468 cells were seeded at a high density in 24-well culture dishes and treated with EGF (50 ng/mL) as previously described for 72 h. Cells were pre-treated with BAPTA-AM (100 μM, 1 h) or NS8593 (1 μM or 10 μM, 24 h). Images were acquired with a Zeiss Axio Observer epifluorescence microscope, using a 20× objective. Regions were selected based on Hoechst nuclear staining.

Immunofluorescence

Immunofluorescence for vimentin was performed as previously described (46). Images were acquired using a 10× objective on an ImageXpress® Micro automated epifluorescence microscope (Molecular Devices) based on the following excitation and emission wavelengths: 377–450 and 447-60 nm for DAPI and 531-40 and 593–640 nm for Cy3-vimentin. Integrated intensity and percent positivity for vimentin were determined using MetaXpress® (v3.1.0.83, Molecular Devices). For analysis of integrated intensity, datasets were imported into AcuityXpress (v2.0, Molecular Devices) and image data were normalized using linear (min-max) scaling as per manufacturer's instructions.

Immunoblotting

Cell extracts were generated using protein lysis buffer supplemented with protease and phosphatase inhibitors (Roche Applied Science, Penzberg, Germany). Gel electrophoresis

was performed using NuPAGE 4–12% gradient Bis-Tris gels with MOPS running buffer (Invitrogen), and transferred to a PVDF membrane. Membranes were blocked using 5% non-fat milk powder in PBS with 0.1% Tween-20 for 1 h. The following antibodies were purchased from Cell Signaling Technology (Danvers, MA, USA): anti-phospho-EGFR (4407), anti-EGFR (2232), anti-phospho-ERK1/2 (9106), anti-ERK1/2 (9102), anti-phospho-Akt (4051), anti-Akt (9272), anti-phospho-STAT3 (9138), anti-STAT3 (9139). The anti-vimentin antibody (V6389) was purchased from Sigma Aldrich. Primary antibodies were diluted 1:1000, with the exception of anti-phospho-ERK1/2 (1:2000) and anti-vimentin (1:750), and incubated at 4°C overnight. The following secondary antibodies were used: anti-mouse HRP-conjugated secondary (170–6516) and anti-rabbit HRP-conjugated secondary (170–6515, BioRad, Hercules, CA, USA) at a 1:10,000 dilution. Images were acquired using a VersaDoc Digital Imaging System (BioRad) and analysed using ImageJ (NIH) as per the gel analysis method outlined in the ImageJ documentation. Protein density was normalized to the β-actin loading control (1:10,000), with the exception of ERK1/2, which has a similar molecular weight to β-actin, precluding its use. Phosphorylated proteins were quantified relative to the respective total protein.

siRNA

We used Dharmacon ON-TARGET*plus* SMARTpool siRNA and Dharmacon siGENOME SMARTpool siRNA (Thermo Scientific, Waltham, MA, USA). DharmaFECT4 transfection reagent was used at a concentration of 0.1 μL/well or 0.2 μL/well for low and high density seeding protocols, respectively. Cells were serum starved 48 h post-transfection and stimulated with EGF. The following Dharmacon On-TARGET*plus* SMARTpool™ siRNAs were used in this study: nontargeting (D-001810-10-05), TRPV3 (L-005263-00-0003), TRPC4 (L-006510-01-0003), TRPC5 (L-006511-00-0003), TRPC6 (L-004192-00-0003), TRPM6 (L-005048-00-0003), TRPM7 (L-005393-00-0005), ORAI1 (L-014998-00-0005). The following Dharmacon siGENOME siRNAs were used: nontargeting (D-001206-14-05) and TRPM7 (M-005393-03-0005).

Real time RT-PCR

Total RNA was isolated and purified using Qiagen RNeasy Plus Mini Kits (74134). Omniscript RT Kits (205111, Qiagen, Hilden, Germany) were used for reverse transcription of RNA, and resulting cDNA was amplified using TaqMan Fast Universal PCR Master Mix (4352042) and TaqMan Gene Expression Assays. Gene Expression Assays used in this study include: vimentin (Hs00185584_m1), Twist (Hs00361186_m1), Snail (Hs00195591_m1), N-cadherin (Hs00983062_m1), CD24 (Hs02379687_s1), CD44 (Hs01075861_m1), and TRPM7 (Hs00292383_m1). Reactions were cycled using a StepOnePlus Real Time RT-PCR instrument (Applied Biosystems, Carlsbad, CA, USA) with universal cycling conditions. Relative quantitation was determined with reference to 18S ribosomal RNA and was analysed using the comparative C_T method (53).

Statistical analysis

Statistical analysis was performed using GraphPad Prism (v5.04 for Windows; GraphPad Software, Inc., La Jolla, CA, USA). Statistical tests used are provided in the figure legends.

Supplementary Material

Refer to Web version on PubMed Central for supplementary material.

REFERENCES

1. Kalluri R, Weinberg RA. The basics of epithelial-mesenchymal transition. J Clin Invest. 2009; 119:1420–1428. [PubMed: 19487818]

2. Zeisberg M, Neilson EG. Biomarkers for epithelial-mesenchymal transitions. J Clin Invest. 2009; 119:1429–1437. [PubMed: 19487819]

3. Nieto MA. The ins and outs of the epithelial to mesenchymal transition in health and disease. Annu Rev Cell Dev Biol. 2011; 27:347–376. [PubMed: 21740232]

4. Polyak K, Weinberg RA. Transitions between epithelial and mesenchymal states: acquisition of malignant and stem cell traits. Nat Rev Cancer. 2009; 9:265–273. [PubMed: 19262571]

5. Prat A, Parker JS, Karginova O, Fan C, Livasy C, Herschkowitz JI, et al. Phenotypic and molecular characterization of the claudin-low intrinsic subtype of breast cancer. Breast Cancer Res. 2010; 12:R68. [PubMed: 20813035]

6. Sarrio D, Rodriguez-Pinilla SM, Hardisson D, Cano A, Moreno-Bueno G, Palacios J. Epithelial-mesenchymal transition in breast cancer relates to the basal-like phenotype. Cancer Res. 2008; 68:989–997. [PubMed: 18281472]

7. Proia TA, Keller PJ, Gupta PB, Klebba I, Jones AD, Sedic M, et al. Genetic predisposition directs breast cancer phenotype by dictating progenitor cell fate. Cell Stem Cell. 2011; 8:149–163. [PubMed: 21295272]

8. DiMeo TA, Anderson K, Phadke P, Fan C, Perou CM, Naber S, et al. A novel lung metastasis signature links Wnt signaling with cancer cell self-renewal and epithelial-mesenchymal transition in basal-like breast cancer. Cancer Res. 2009; 69:5364–5373. [PubMed: 19549913]

9. Mani SA, Guo W, Liao M-J, Eaton EN, Ayyanan A, Zhou AY, et al. The epithelial-mesenchymal transition generates cells with properties of stem cells. Cell. 2008; 133:704–715. [PubMed: 18485877]

10. Creighton CJ, Li X, Landis M, Dixon JM, Neumeister VM, Sjolund A, et al. Residual breast cancers after conventional therapy display mesenchymal as well as tumor-initiating features. Proc Natl Acad Sci U S A. 2009; 106:13820–13825. [PubMed: 19666588]

11. Thiery JP, Acloque H, Huang RYJ, Angela Nieto M. Epithelial-mesenchymal transitions in development and disease. Cell. 2009; 139:871–890. [PubMed: 19945376]

12. Hugo H, Ackland ML, Blick T, Lawrence MG, Clements JA, Williams ED, et al. Epithelial-mesenchymal and mesenchymal - Epithelial transitions in carcinoma progression. J Cell Physiol. 2007; 213:374–383. [PubMed: 17680632]

13. Lo H-W, Hsu S-C, Xia W, Cao X, Shih J-Y, Wei Y, et al. Epidermal growth factor receptor cooperates with signal transducer and activator of transcription 3 to induce epithelial-mesenchymal transition in cancer cells via up-regulation of TWIST gene expression. Cancer Res. 2007; 67:9066–9076. [PubMed: 17909010]

14. Berg T. Inhibition of transcription factors with small organic molecules. Curr Opin Chem Biol. 2008; 12:464–471. [PubMed: 18706517]

15. Berridge MJ, Bootman MD, Roderick HL. Calcium signalling: Dynamics, homeostasis and remodelling. Nat Rev Mol Cell Biol. 2003; 4:517–529. [PubMed: 12838335]

16. Ronnov-Jessen L, Bissell MJ. Breast cancer by proxy: can the microenvironment be both the cause and consequence? Trends Mol Med. 2009; 15:5–13. [PubMed: 19091631]

17. Monteith GR, Davis FM, Roberts-Thompson SJ. Calcium channels and pumps in cancer: changes and consequences. J Biol Chem. 2012; 287:31666–31673. [PubMed: 22822055]

18. Yang SL, Cao Q, Zhou KC, Feng YJ, Wang YZ. Transient receptor potential channel C3 contributes to the progression of human ovarian cancer. Oncogene. 2009; 28:1320–1328. [PubMed: 19151765]

19. Prevarskaya N, Skryma R, Shuba Y. Calcium in tumour metastasis: new roles for known actors. Nat Rev Cancer. 2011; 11:609–618. [PubMed: 21779011]

20. Monet M, Lehen'kyi Vy, Gackiere F, Firlej V, Vandenberghe M, Roudbaraki M, et al. Role of cationic channel TRPV2 in promoting prostate cancer migration and progression to androgen resistance. Cancer Res. 2010; 70:1225–1235. [PubMed: 20103638]

21. Yang S, Zhang JJ, Huang X-Y. Orai1 and STIM1 are critical for breast tumor cell migration and metastasis. Cancer Cell. 2009; 15:124–134. [PubMed: 19185847]

22. Davis FM, Peters AA, Grice DM, Cabot PJ, Parat MO, Roberts-Thomson SJ, et al. Non-stimulated, agonist-stimulated and store-operated Ca2+ influx in MDA-MB-468 breast cancer cells and the effect of EGF-induced EMT on calcium entry. PLoS ONE. 2012; 7:e36923. [PubMed: 22666335]

23. Hu JJ, Qin KH, Zhang Y, Gong JB, Li N, Lv D, et al. Downregulation of transcription factor Oct4 induces an epithelial-to-mesenchymal transition via enhancement of Ca(2+) influx in breast cancer cells. Biochem Biophys Res Commun. 2011; 411:786–791. [PubMed: 21798248]

24. Gilles C, Polette M, Zahm JM, Tournier JM, Volders L, Foidart JM, et al. Vimentin contributes to human mammary epithelial cell migration. J Cell Sci. 1999; 112:4615–4625. [PubMed: 10574710]

25. Bonnomet A, Syne L, Brysse A, Feyereisen E, Thompson EW, Noel A, et al. A dynamic in vivo model of epithelial-to-mesenchymal transitions in circulating tumor cells and metastases of breast cancer. Oncogene. 2011; 31:3741–3753. [PubMed: 22120722]

26. Wyckoff J, Wang WG, Lin EY, Wang YR, Pixley F, Stanley ER, et al. A paracrine loop between tumor cells and macrophages is required for tumor cell migration in mammary tumors. Cancer Res. 2004; 64:7022–7029. [PubMed: 15466195]

27. Berridge MJ, Lipp P, Bootman MD. The versatility and universality of calcium signalling. Nat Rev Mol Cell Biol. 2000; 1:11–21. [PubMed: 11413485]

28. Ji QS, Carpenter G. Role of basal calcium in the EGF activation of MAP kinases. Oncogene. 2000; 19:1853–1856. [PubMed: 10777220]

29. Cook SJ, Beltman J, Cadwallader KA, McMahon M, McCormick F. Regulation of mitogen-activated protein kinase phosphatase-1 expression by extracellular signal-related kinase-dependent and Ca2+-dependent signal pathways in Rat-1 cells. J Biol Chem. 1997; 272:13309–13319. [PubMed: 9148952]

30. Colomiere M, Ward AC, Riley C, Trenerry MK, Cameron-Smith D, Findlay J, et al. Cross talk of signals between EGFR and IL-6R through JAK2/STAT3 mediate epithelial-mesenchymal transition in ovarian carcinomas. Br J Cancer. 2009; 100:134–144. [PubMed: 19088723]

31. Wei C, Wang X, Chen M, Ouyang K, Song L-S, Cheng H. Calcium flickers steer cell migration. Nature. 2009; 457:901–905. [PubMed: 19118385]

32. Cheng X, Jin J, Hu L, Shen D, Dong X-p, Samie MA, et al. TRP channel regulates EGFR signaling in hair morphogenesis and skin barrier formation. Cell. 2010; 141:331–343. [PubMed: 20403327]

33. Gao H, Chen X, Du X, Guan B, Liu Y, Zhang H. EGF enhances the migration of cancer cells by up-regulation of TRPM7. Cell Calcium. 2011; 50:559–568. [PubMed: 21978419]

34. Middelbeek J, Kuipers AJ, Henneman L, Visser D, Eidhof I, van Horssen R, et al. TRPM7 is required for breast tumor cell metastasis. Cancer Res. 2012; 72:4250–4261. [PubMed: 22871386]

35. Chubanov V, Mederos y Schnitzler M, Meissner M, Schafer S, Abstiens K, Hofmann T, et al. Natural and synthetic modulators of SK (K(ca)2) potassium channels inhibit magnesium-

dependent activity of the kinase-coupled cation channel TRPM7. Br J Pharmacol. 2012; 166:1357–1376. [PubMed: 22242975]

36. Langeslag M, Clark K, Moolenaar WH, van Leeuwen FN, Jalink K. Activation of TRPM7 channels by phospholipase C-coupled receptor agonists. J Biol Chem. 2007; 282:232–239. [PubMed: 17095511]

37. Ramsey IS, Delling M, Clapham DE. An introduction to TRP channels. Annu Rev Physiol. 2006; 68:619–647. [PubMed: 16460286]

38. Shabir S, Southgate J. Calcium signalling in wound-responsive normal human urothelial cell monolayers. Cell Calcium. 2008; 44:453–464. [PubMed: 18417211]

39. Chang HY, Nuyten DSA, Sneddon JB, Hastie T, Tibshirani R, Sorlie T, et al. Robustness, scalability, and integration of a wound-response gene expression signature in predicting breast cancer survival. Proc Natl Acad Sci U S A. 2005; 102:3738–3743. [PubMed: 15701700]

40. Grande M, Franzen A, Karlsson JO, Ericson LE, Heldin NE, Nilsson M. Transforming growth factor-beta and epidermal growth factor synergistically stimulate epithelial to mesenchymal transition (EMT) through a MEK-dependent mechanism in primary cultured pig thyrocytes. J Cell Sci. 2002; 115:4227–4236. [PubMed: 12376555]

41. Su LT, Liu W, Chen HC, Gonzalez-Pagan O, Habas R, Runnels LW. TRPM7 regulates polarized cell movements. Biochem J. 2011; 434:513–521. [PubMed: 21208190]

42. Takahashi T, Fukuda K, Pan J, Kodama H, Sano M, Makino S, et al. Characterization of insulin-like growth factor-1-induced activation of the JAK/STAT pathway in rat cardiomyocytes. Circ Res. 1999; 85:884–891. [PubMed: 10559134]

43. Vultur A, Cao J, Arulanandam R, Turkson J, Jove R, Greer P, et al. Cell-to-cell adhesion modulates Stat3 activity in normal and breast carcinoma cells. Oncogene. 2004; 23:2600–2616. [PubMed: 15007380]

44. Mellstrom B, Savignac M, Gomez-Villafuertes R, Naranjo JR. Ca2+-operated transcriptional networks: Molecular mechanisms and in vivo models. Physiol Rev. 2008; 88:421–449. [PubMed: 18391169]

45. Mancini M, Toker A. NFAT proteins: emerging roles in cancer progression. Nat Rev Cancer. 2009; 9:810–820. [PubMed: 19851316]

46. Davis FM, Kenny PA, Soo ETL, van Denderen BJW, Thompson EW, Cabot PJ, et al. Remodeling of purinergic receptor-mediated Ca(2+) signaling as a consequence of EGF-induced epithelial-mesenchymal transition in breast cancer cells. PLoS ONE. 2011; 6:e23464. [PubMed: 21850275]

47. Clark K, Langeslag M, van Leeuwen B, Ran L, Ryazanov AG, Figdor CG, et al. TRPM7, a novel regulator of actomyosin contractility and cell adhesion. EMBO J. 2006; 25:290–301. [PubMed: 16407977]

48. Lundgren K, Nordenskjold B, Landberg G. Hypoxia, Snail and incomplete epithelial-mesenchymal transition in breast cancer. Br J Cancer. 2009; 101:1769–1781. [PubMed: 19844232]

49. Lester RD, Jo M, Montel V, Takimoto S, Gonias SL. uPAR induces epithelial-mesenchymal transition in hypoxic breast cancer cells. J Cell Biol. 2007; 178:425–436. [PubMed: 17664334]

50. Liang C-C, Park AY, Guan J-L. In vitro scratch assay: a convenient and inexpensive method for analysis of cell migration in vitro. Nat Protoc. 2007; 2:329–333. [PubMed: 17406593]

51. Elgoyhen AB, Vetter DE, Katz E, Rothlin CV, Heinemann SF, Boulter J. alpha 10: A determinant of nicotinic cholinergic receptor function in mammalian vestibular and cochlear mechanosensory hair cells. Proc Natl Acad Sci U S A. 2001; 98:3501–3506. [PubMed: 11248107]

52. Grice DM, Vetter I, Faddy HM, Kenny PA, Roberts-Thomson SJ, Monteith GR. Golgi calcium pump secretory pathway calcium ATPase 1 (SPCA1) is a key regulator of insulin-like growth factor receptor (IGF1R) processing in the basal-like breast cancer cell line MDA-MB-231. J Biol Chem. 2010; 285:37458–37466. [PubMed: 20837466]

53. Suchanek KM, May FJ, Robinson JA, Lee WJ, Holman NA, Monteith GR, et al. Peroxisome proliferator-activated receptor alpha in the human breast cancer cell lines MCF-7 and MDA-MB-231. Mol Carcinog. 2002; 34:165–171. [PubMed: 12203367]
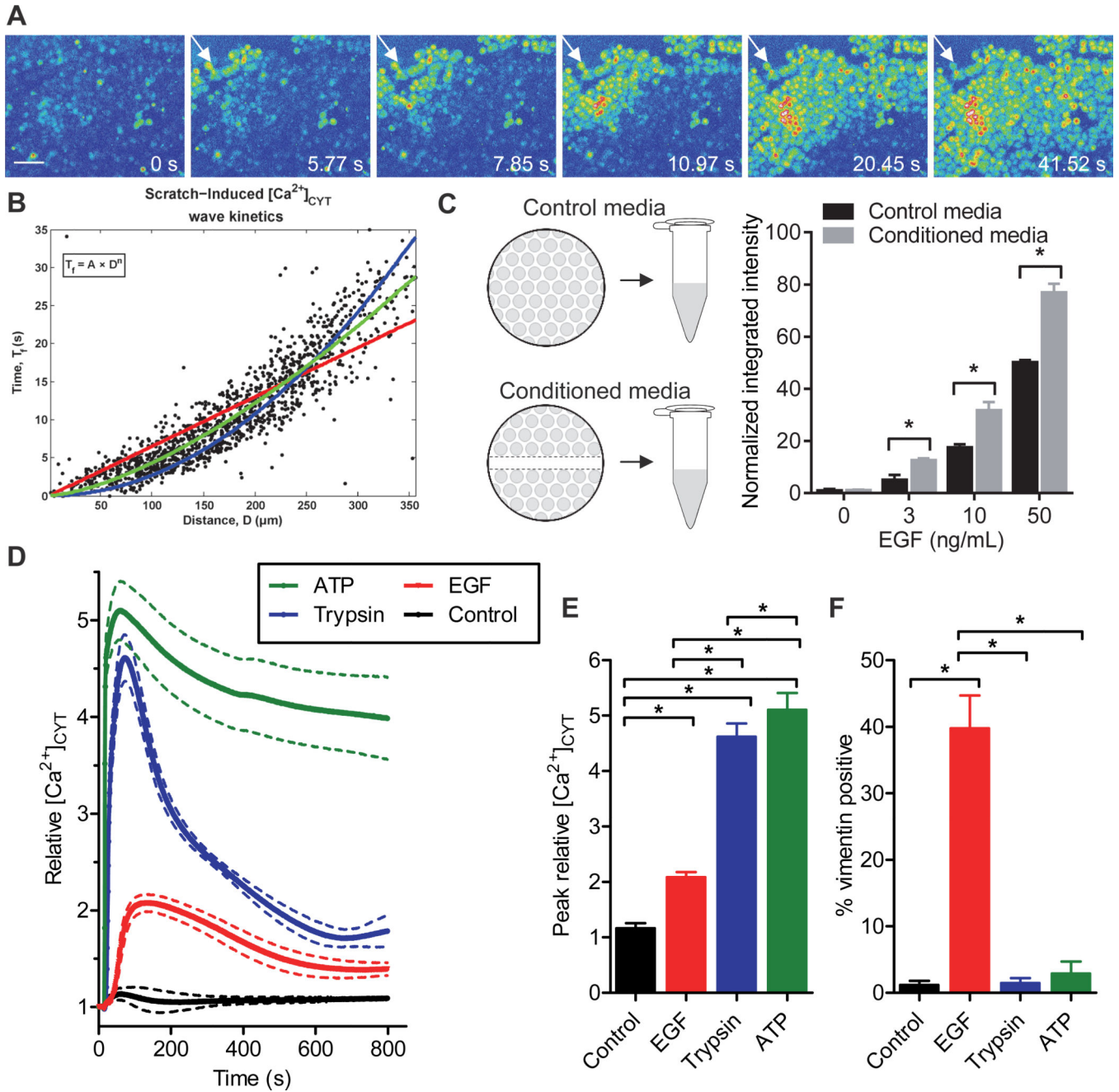
Figure 1. Stimuli known to induce EMT produce a transient increase in cytosolic calcium
A) Pseudocolor (intensity) representation of calcium wave propagation through a confluent monolayer of MDA-MB-468 cells loaded with Fluo-4 AM calcium indicator. White arrows indicate the wound edge. Scale bar, 75 μm. Representative of movies from three independent experiments. **B**) Scatter plots for all frames of all movies showing cell activation time (T_f) versus distance (D) from the wound edge during scratch-induced calcium wave propagation; A represents the scaling coefficient and n the power law exponent, used to estimate the mode of activation. An n of 1 (red) represents calcium wave propagation that more closely resembles intercellular communication, whilst an n of 2 (blue)

signifies activation by the release of a diffusible extracellular factor. The green line indicates the line of best-fit for scratch-induced calcium wave propagation. See also Fig. S1 and Movie S1. **C**) MDA-MB-468 cells were incubated for 30 min with conditioned media (the supernatant of a wounded monolayer) prior to stimulation with EGF (24 h) and vimentin protein expression was assessed using immunofluorescence. Two-way ANOVA with Bonferroni's multiple comparisons post-tests was used to assess the significance of conditioned media at each EGF concentration. **D**) Average relative $[Ca^{2+}]_{CYT}$ transients, **E**) peak relative $[Ca^{2+}]_{CYT}$ response and **F**) vimentin positivity in cells stimulated with ATP (100 μM), trypsin (30 nM) or EGF (50 ng/mL). Bar graphs show mean ± S.D. for nine individual wells from three independent experiments. Significance was assessed using one-way ANOVA with Bonferroni's multiple comparisons post-tests. * $P < 0.05$.
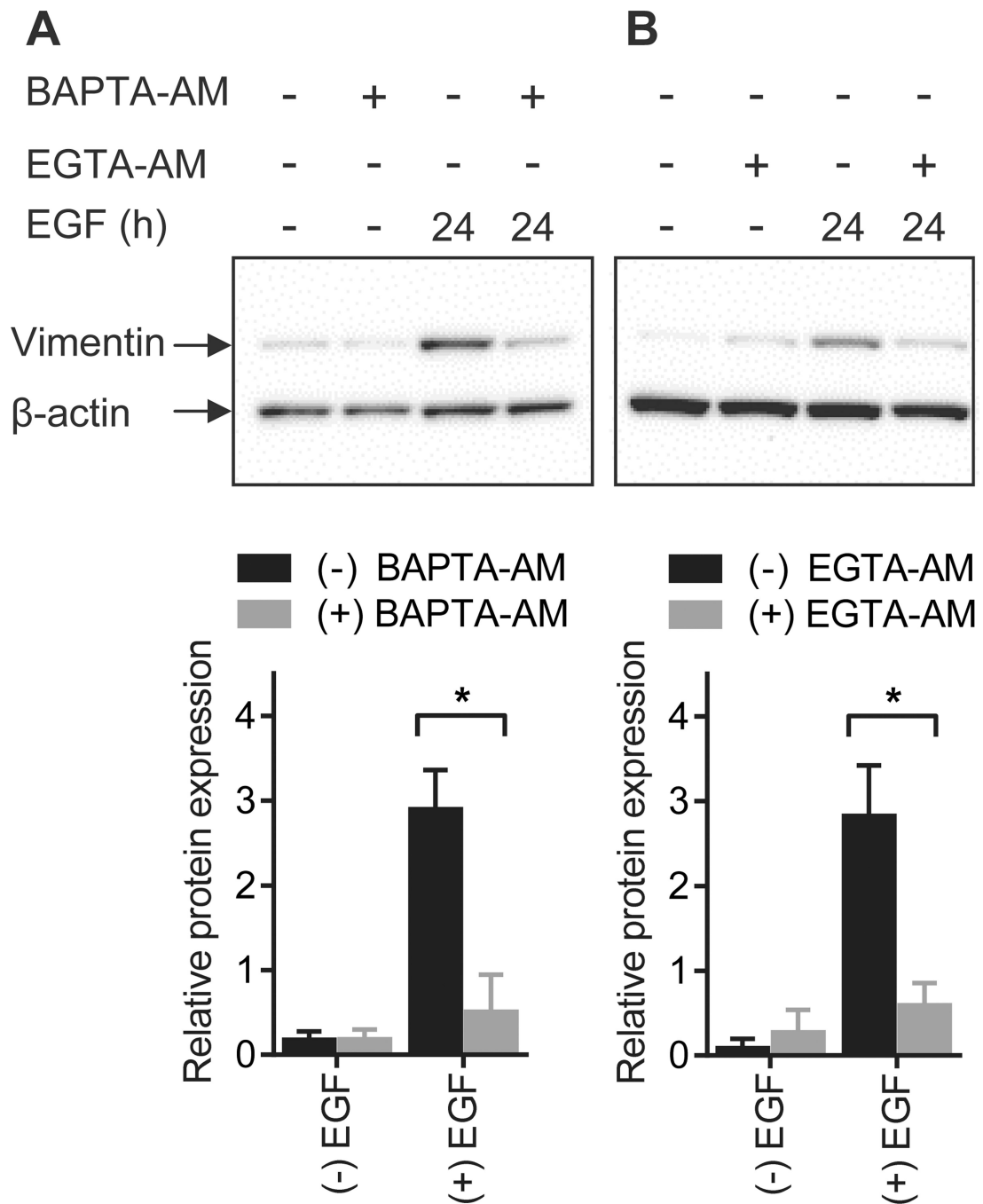
Figure 2. Calcium regulates EGF-induced vimentin protein expression
Representative immunoblots and densitometric analysis (normalized to β-actin) of EGF-induced vimentin expression in breast cancer cells loaded with **A**) BAPTA-AM or **B**) EGTA-AM to block increases in cytosolic calcium levels. Bar graphs show mean ± S.D. for three independent experiments. The effect of calcium chelation on vimentin expression was assessed using two-way ANOVA with Bonferroni's multiple comparisons post-tests. * $P <$ 0.05.
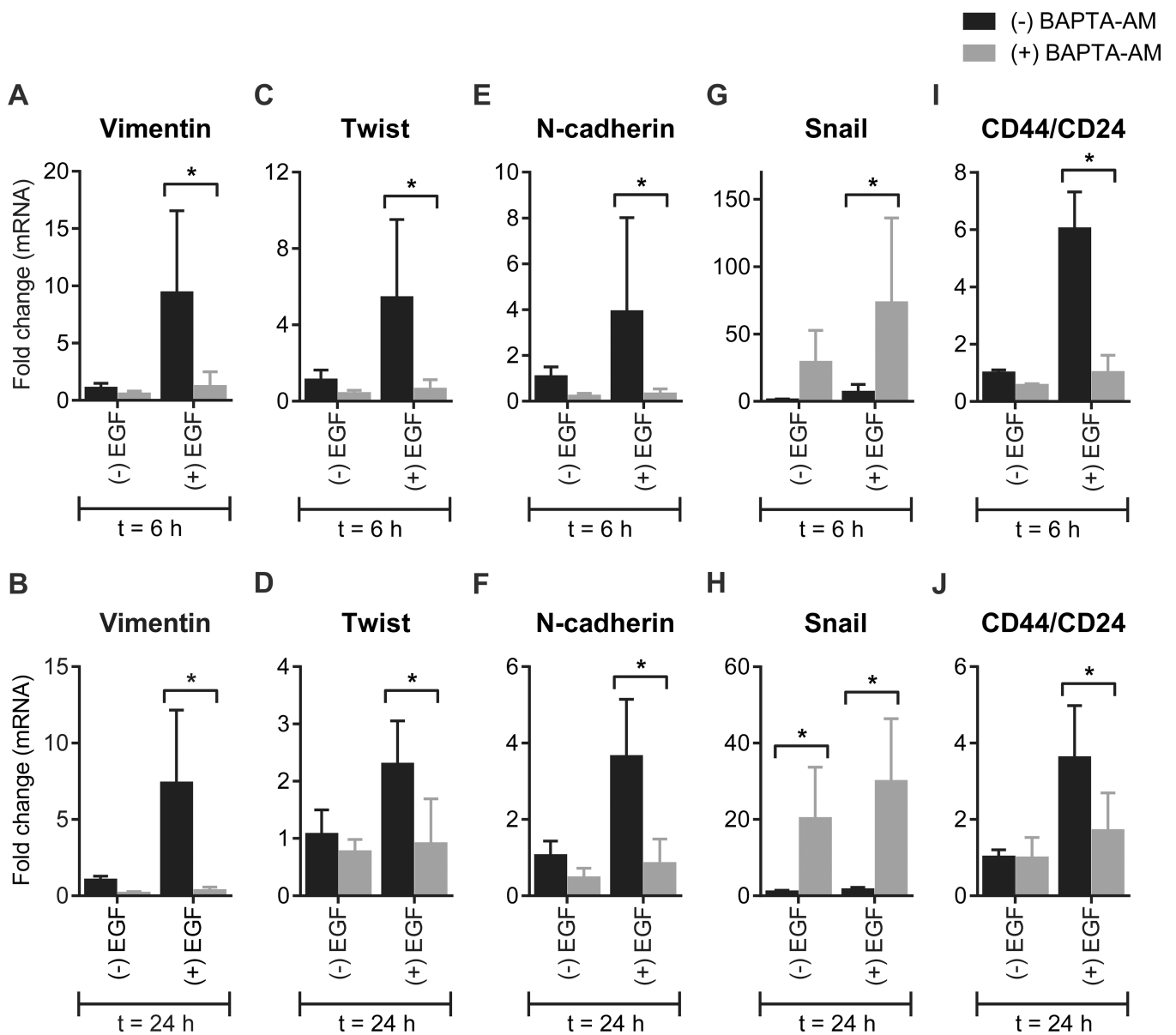
Figure 3. Calcium regulates the induction of some genes implicated in EGF-induced EMT

Analysis of mRNA levels of EMT-associated genes (vimentin, Twist, N-cadherin, Snail and CD44/CD24) in MDA-MB-468 breast cancer cells with intracellular calcium chelation (BAPTA-AM). Cells were treated with EGF for 6 h (**A, C, E, G and I**) or 24 h (**B, D, F, H and J**) to induce EMT. Bar graphs show mean ± S.D. for nine individual wells from three independent experiments. The effect of BAPTA-AM on gene expression was assessed using two-way ANOVA with Bonferroni's multiple comparisons post-tests. * $P < 0.05$.
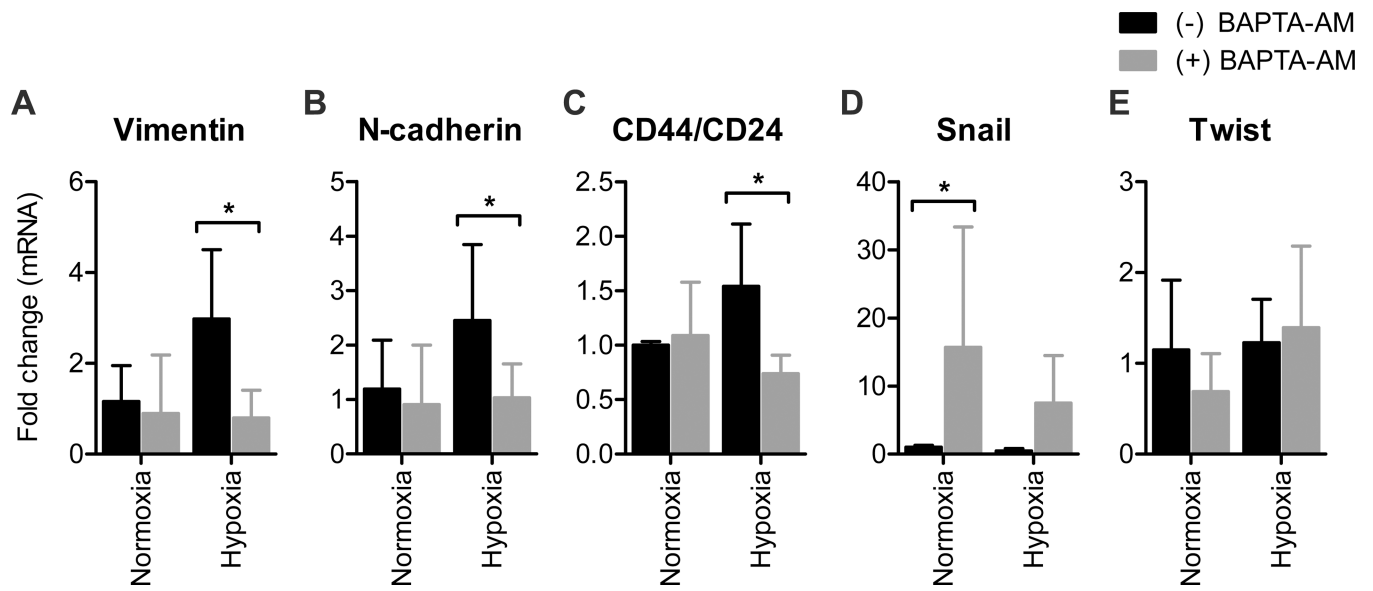
Figure 4. Calcium regulates the induction of some genes implicated in hypoxia-mediated EMT
Assessment of mRNA levels of **A**) vimentin, **B**) N-cadherin, **C**) CD44/CD24, **D**) Snail and
E) Twist with normoxia or hypoxia (1% O_2) in MDA-MB-468 breast cancer cells with
intracellular calcium chelation (BAPTA-AM). Bar graphs show mean ± S.D. for nine
individual wells from three independent experiments. The effect of BAPTA-AM on gene
expression was assessed using two-way ANOVA with Bonferroni's multiple comparisons
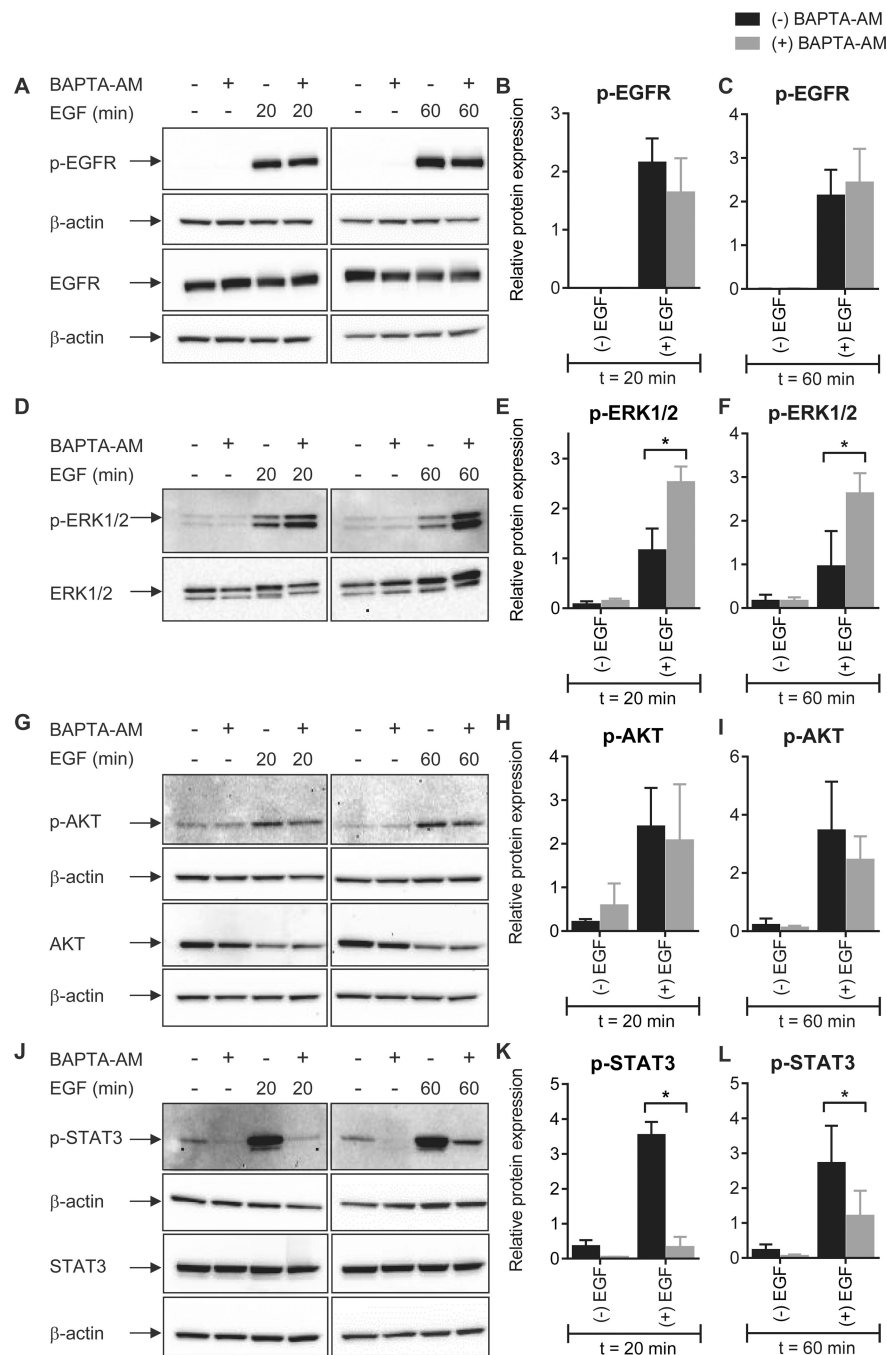post-tests. * $P < 0.05$.

Figure 5. The effect of intracellular calcium chelation on EGFR phosphorylation and activation of downstream signal transduction pathways

Phosphorylation of EGFR (Tyr1173) (**A–C**), ERK1/2 (Thr202/Tyr204) (**D–F**), Akt (Ser473) (**G–I**) and STAT3 (Tyr705) (**J–L**) mediated by incubation with 50 ng/mL EGF for 20 or 60 min was assessed in cells with intracellular calcium chelation (BAPTA-AM). Bar graphs show mean ± S.D. for three independent experiments. The effect of calcium chelation on protein phosphorylation was assessed using two-way ANOVA with Bonferroni's multiple comparisons post-tests. * $P < 0.05$.
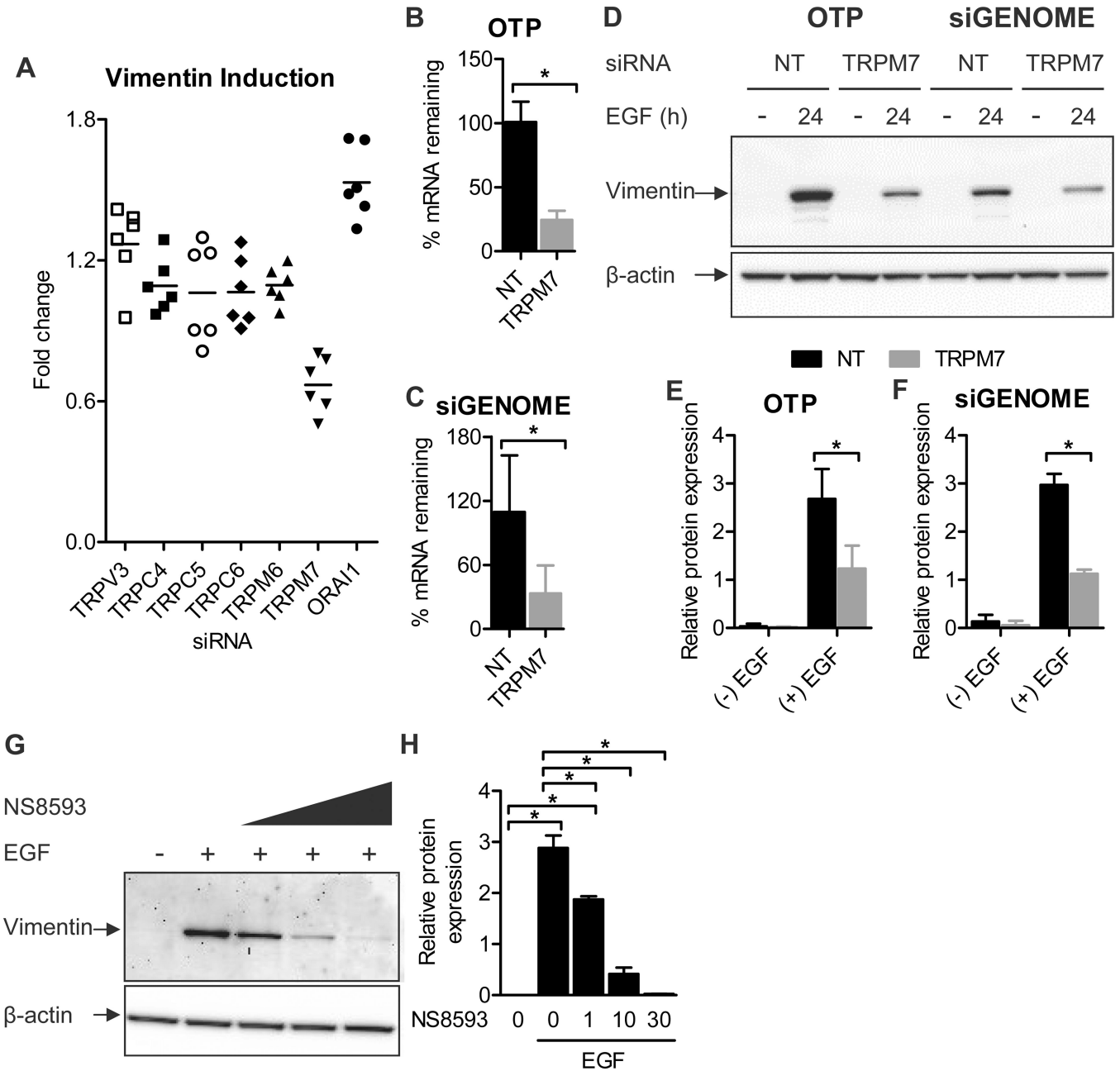
Figure 6. siRNA silencing and pharmacological inhibition of TRPM7 inhibit EGF-induced vimentin protein expression

A) TRPV3, TRPC4, TRPC5, TRPC6, TRPM6, TRPM7 and ORAI1 calcium-permeable channels were silenced using Dharmacon ON-TARGET*plus* siRNA and cells were stimulated with EGF (10 ng/mL, 24 h). Vimentin protein expression (integrated intensity) was assessed with quantitative immunofluorescence. The scatter dot plot shows fold change relative to the non-targeting (NT) control for six individual wells from two independent experiments. Analysis of percent TRPM7 mRNA remaining following transfection with **B**) Dharmacon ON-TARGET*plus* (OTP) TRPM7 siRNA or **C**) Dharmacon siGENOME TRPM7 siRNA. Bar graphs show mean ± S.D. for six wells from two independent

experiments. Statistical significance was assessed using a student's t-test. **D**) Representative immunoblot confirming regulation by TRPM7 of EGF-induced vimentin expression and densitometric analysis of vimentin expression (normalized to β-actin) in cells transfected with **E**) OTP TRPM7 siRNA or **F**) siGENOME TRPM7 siRNA. Graphs show mean ± S.D. for three independent experiments. The effect of TRPM7 gene silencing on vimentin expression was assessed using two-way ANOVA with Bonferroni's multiple comparisons post-tests. **G**) Representative immunoblot showing the effect of increasing concentrations of the TRPM7 inhibitor NS8593 on EGF-induced vimentin expression and **H**) densitometric analysis (normalized to β-actin) for three independent experiments. Cells were treated with NS8593 for 24 h prior to EGF treatment and NS8593 was maintained during EGF treatment. Statistical significance was assessed using one-way ANOVA with Bonferroni's multiple comparisons post-tests. * $P < 0.05$.
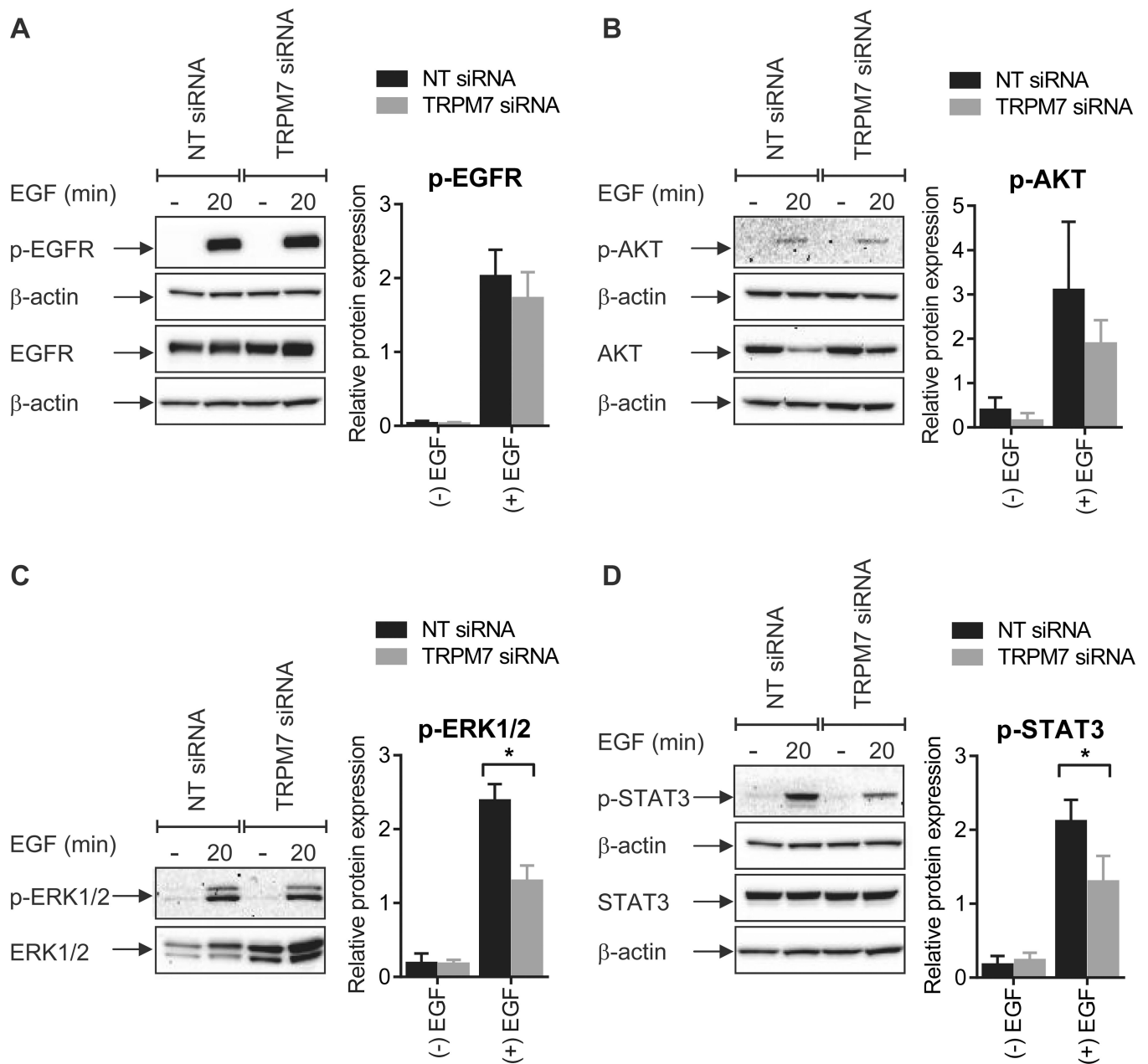
Figure 7. TRPM7 silencing alters specific EGF signaling pathways
Phosphorylation of **A**) EGFR (Tyr1173), **B**) Akt (Ser473), **C**) ERK1/2 (Thr202/Tyr204), and **D**) STAT3 (Tyr705) following EGF stimulation (50 ng/mL, 20 min) in MDA-MB-468 breast cancer cells transfected with nontargeting (NT) siRNA or TRPM7 OTP siRNA. Graphs show mean ± S.D. for three independent experiments. The effect of TRPM7 gene silencing on protein phosphorylation was assessed using two-way ANOVA with Bonferroni's multiple comparisons post-tests. * $P < 0.05$.